Syntheses, Structure, Magnetism, and Optical Properties of Lutetium-based Interlanthanide Selenides

Geng Bang Jin,[†] Eun Sang Choi,[‡] Robert P. Guertin,[§] James S. Brooks,[‡]

Corwin H. Booth,[£] and Thomas E. Albrecht-Schmitt[†,*]

[†]Department of Chemistry and Biochemistry and the E. C. Leach Nuclear Science Center, Auburn University, Auburn, Alabama 36849

[‡]Department of Physics and National High Magnetic Field Laboratory, Florida State University, Tallahassee, Florida 32310

[§]Department of Physics and Astronomy, Tufts University, Medford, Massachusetts 02155

[£]Chemical Sciences Division, Lawrence Berkeley National Laboratory, 1 Cyclotron Rd., Berkeley, CA 94720

Published in Inorg. Chem. ***46****, 9213 (2007).*

Abstract

Ln_3LuSe_6 (Ln = La, Ce), β-$LnLuSe_3$ (Ln = Pr, Nd), and $Ln_xLu_{4-x}Se_6$ (Ln = Sm, Gd; x = 1.82, 1.87) have been synthesized using a Sb_2Se_3 flux at 1000 °C. Ln_3LuSe_6 (Ln = La, Ce) adopt the U_3ScS_6-type three-dimensional structure, which is constructed from two-dimensional $^{2}_{\infty}[Ln_3Se_6]^{3-}$ slabs with the gaps between these slabs filled by octahedrally coordinated Lu^{3+} ions. The series of β-$LnLuSe_3$ (Ln = Pr, Nd) are isotypic with $UFeS_3$. Their structures include layers formed from $LuSe_6$ octahedra that are separated by eight-coordinate larger Ln^{3+} ions in bicapped trigonal prismatic environments. $Sm_{1.82}Lu_{2.18}Se_6$ and $Gd_{1.87}Lu_{2.13}Se_6$ crystallize in the disordered F-Ln_2S_3 type structure with the eight-coordinate bicapped trigonal prismatic Ln(1) ions residing in the one-dimensional channels formed by three different double chains via edge and corner sharing. These double chains are constructed from $Ln(2)Se_7$ monocapped trigonal prisms, $Ln(3)Se_6$ octahedra, and $Ln(4)S_6$ octahedra, respectively. The magnetic susceptibilities of β-$PrLuSe_3$ and β-$NdLuSe_3$ follow the Curie-Weiss law. $Sm_{1.82}Lu_{2.18}Se_6$ shows van Vleck paramagnetism. Magnetic measurements show that $Gd_{1.87}Lu_{2.13}Se_6$ undergoes an antiferromagnetic transition around 4 K. Ce_3LuSe_6 exhibits ferromagnetic ordering below 5 K. The optical band gaps for La_3LuSe_6, Ce_3LuSe_6, β-$PrLuSe_3$, β-$NdLuSe_3$, $Sm_{1.82}Lu_{2.18}Se_6$, and $Gd_{1.87}Lu_{2.13}Se_6$ are 1.26, 1.10, 1.56, 1.61, 1.51, and 1.56 eV, respectively.

Introduction

Interlanthanide chalcogenides have been the focus of intense interest owing to their remarkably complex structures, tunable band gaps, and in some cases atypical magnetism.[1-21] New developments in this area have been aided by the use of fluxes for the synthesis and crystal growth of new compounds. These fluxes have included a variety of alkali metal halides as well as Sb_2Q_3 (Q = S, Se).[14,15,20-22]

Ternary interlanthanide chalcogenides usually include one large ion (Ln) and one small ion (Ln') that are from both ends of lanthanide series with different coordination environments to avoid possible disordering. Ln/Yb/Q (Q = S, Se) phases have been extensively studied owing to the potential mixed-valency of Yb (II, III) ions, which might lead to interesting structures and electronic properties. The group of Ln/Yb/Q (Q = S, Se) is represented by α-$LaYbS_3$[12] ($GdFeO_3$ type [19]),[23] β-$LnYbQ_3$ (Q = S, Se)[12-14] ($UFeS_3$ type),[24] γ-$LnYbS_3$ (Ln = La, Ce),[15] and $LnYb_3S_6$[16,17] (F-Ln_2S_3 type).[25,26] There are some Er or Tm containing ternary compounds prepared and characterized, including $CeTmS_3$,[18] $La_{10}Er_9S_{27}$,[19] γ-$LnLn'S_3$ (Ln = La, Ce; Ln' = Er, Tm),[15] $SmEr_3Q_6$ (Q = S, Se)[20] (F-Ln_2S_3 type),[25,26] and $Sm_{0.88}Er_{1.12}Se_3$[20] (U_2S_3 type).[27] Both Er^{3+} and Tm^{3+} ions are paramagnetic. Their substitutions in smaller Ln' sites may result in different magnetic performance from the parent compounds. In contrast, Ln/Lu/Q phases are much simpler systems in term of magnetism and less investigated, because the Lu^{3+} ion is $4f^{14}$. The full 4f shell of the Lu^{3+} ion can be advantageous when the magnetic behavior of other Ln ions needs to be probed without the interference from Ln' ions.

Recently, we reported the synthesis and characterization of interlanthanide sulfides δ-$Ln_{2-x}Lu_xS_3$ (Ln = Ce, Pr, Nd).[21] These compounds crystallized in the disordered $CeTmS_3$ structure-type with tunable band gaps. The magnetic susceptibility of

δ-$Ce_{1.30}Lu_{0.70}S_3$ deviates from the Curie-Weiss law at low temperature, due to the crystal-field effects**.** δ-$Pr_{1.29}Lu_{0.71}S_3$ shows some short-range antiferromagnetic ordering. While δ-$Nd_{1.33}Lu_{0.67}S_3$ acts like an intermediate state of δ-$Ce_{1.30}Lu_{0.70}S_3$ and δ-$Pr_{1.29}Lu_{0.71}S_3$. In the present study, we disclose the synthesis, structure, optical, and magnetic properties of Ln_3LuSe_6 (Ln = La, Ce), β-$LnLuSe_3$ (Ln = Pr, Nd), and $Ln_xLu_{4-x}Se_6$ (Ln = Sm, Gd; x = 1.82, 1.87).

Experimental

Starting Materials. La (99.9%, Alfa-Aesar), Ce (99.9%, Alfa-Aesar), Pr (99.9%, Alfa-Aesar), Nd (99.9%, Alfa-Aesar), Sm (99.9%, Alfa-Aesar), Gd (99.9%, Alfa-Aesar), Lu (99.9%, Alfa-Aesar), Se (99.5%, Alfa-Aesar), and Sb (99.5%, Alfa-Aesar) were used as received. The Sb_2Se_3 flux was prepared from the direct reaction of the elements in sealed fused-silica ampoules at 850 °C.

Syntheses. Ln_3LuSe_6 (Ln = La, Ce) were synthesized from a reaction of 150 mg of stoichiometric Ln, Lu, and Se, and 100 mg of Sb_2Se_3. For β-$LnLuSe_3$ (Ln = Pr, Nd) and $Ln_xLu_{4-x}Se_6$ (Ln = Sm, Gd; x = 1.82, 1.87), the reaction mixtures include 150 mg of Ln, Lu, and Se in a molar ratio of 1:1:3, and 100 mg of Sb_2Se_3. All these starting materials were loaded into fused-silica ampoules under argon atmosphere in a glovebox. The ampoules were frame sealed under vacuum and heated in programmable tube furnaces. The following heating profile was used for all reactions: 2 °C/min to 500 °C (held for 1 h), 0.5 °C/min to 1000 °C (held for 14 d), 0.04 °C/min to 550 °C (held for 2 d), and 0.5 °C/min to 24 °C. Major title products were found as large black chunks that were well separated from the Sb_2Se_3 flux. They were isolated and ground for powder X-ray

diffraction measurements, which were used to confirm phase purity by comparing the powder patterns calculated from the single crystal X-ray structures with the experimental data. Semi-quantitative SEM/EDX analyses were performed on several single crystals for each compound using a JEOL 840/Link Isis or JEOL JSM-7000F instruments. Ln, Lu, and Se percentages were calibrated against standards. Sb was not detected in the crystals. The Ln:Lu:Se ratios for Ln_3LuSe_6 (Ln = La, Ce) were determined to be approximately 3:1:6 from EDX analyses. While the ratios of Ln:Lu:Se were close to 1:1:3 for β-$LnLuSe_3$ (Ln = Pr, Nd) and $Ln_xLu_{4-x}Se_6$ (Ln = Sm, Gd; x = 1.82, 1.87).

Crystallographic Studies. Single crystals of $Ln_xLu_ySe_z$ (Ln = La, Ce, Pr, Nd, Sm, Gd) were mounted on glass fibers with epoxy and optically aligned on a Bruker APEX single crystal X-ray diffractometer using a digital camera. Initial intensity measurements were performed using graphite monochromated Mo Kα (λ = 0.71073 Å) radiation from a sealed tube and monocapillary collimator. SMART (v 5.624) was used for preliminary determination of the cell constants and data collection control. The intensities of reflections of a sphere were collected by a combination of 3 sets of exposures (frames). Each set had a different ϕ angle for the crystal and each exposure covered a range of 0.3° in ω. A total of 1800 frames were collected with exposure times per frame of 10 or 20 seconds depending on the crystal.

For $Ln_xLu_ySe_z$ (Ln = La, Ce, Pr, Nd, Sm, Gd), determination of integrated intensities and global refinement were performed with the Bruker SAINT (v 6.02) software package using a narrow-frame integration algorithm. These data were treated first with a face-index numerical absorption correction using XPREP,[28] followed by a semi-empirical absorption correction using SADABS.[29] The program suite SHELXTL (v

6.12) was used for space group determination (XPREP), direct methods structure solution (XS), and least-squares refinement (XL).[28] The final refinements included anisotropic displacement parameters for all atoms and secondary extinction. Some crystallographic details are given in Table 1. Additional crystallographic information can be found in the Supporting Information.

The structures of Ln_3LuSe_6 (Ln = La, Ce) and β-$LnLuSe_3$ (Ln = Pr, Nd) are ordered. For these compounds, the assignments of cation positions were straightforward. $Ln_xLu_{4-x}Se_6$ (Ln = Sm, Gd; x = 1.82, 1.87) compounds crystallize in F-Ln_2S_3[25,26] type structure, which is highly disordered. All four cation sites, including one eight-coordinate position (Ln (1)), one seven-coordinate position (Ln (2)), and two octahedral positions (Ln (3) and Ln (4)), were assumed to be occupied by both metals at the beginning of the refinements. The final refinements shown that the occupancies of Lu atoms in Ln (1), Ln (2), Ln (3), and Ln (4) positions are 0.02, 0.32, 0.88, and 0.95 respectively for Sm-based compound and 0.04, 0.40, 0.084 and 0.086 for Gd case. These results gave rise to the formula of $Sm_{1.82}Lu_{2.18}Se_6$ and $Gd_{1.87}Lu_{2.13}Se_6$, which are consistent with the 1:1:3 ratios from EDX analysis. It is worth to note that $Gd_{1.87}Lu_{2.13}Se_6$ has higher degree of disorder than $Sm_{1.82}Lu_{2.18}Se_6$ as the size of the cations getting closer, even though they have similar Ln:Lu ratios.

Powder X-ray Diffraction. Powder X-ray diffraction patterns were collected with a Rigaku Miniflex powder X-ray diffractometer using Cu Kα (λ = 1.54056 Å) radiation.

Magnetic Susceptibility Measurements. Magnetism data were measured on powders in gelcap sample holders with a Quantum Design MPMS 7T

magnetometer/susceptometer between 2 and 300 K and in applied fields up to 7 T. DC susceptibility measurements were made under zero-field-cooled conditions with an applied field of 0.1 T. Magnetic susceptibility for Ce_3LuSe_6 under zero-field-cooled (ZFC) and field-cooled (FC) conditions were measured with 0.01 T applied field between 2 and 25 K. Susceptibility values were corrected for the sample diamagnetic contribution according to Pascal's constants[30] as well as for the sample holder diamagnetism. Experimental effective magnetic moments and Weiss constants for Ce_3LuSe_6, β-$PrLuSe_3$, β-$NdLuSe_3$, and $Gd_{1.87}Lu_{2.13}Se_6$ were obtained from extrapolations from fits between 100 and 300 K.

UV-vis-NIR Diffuse Reflectance Spectroscopy. The diffuse reflectance spectra for $Ln_xLu_ySe_z$ (Ln = La, Ce, Pr, Nd, Sm, Gd) were measured from 200 to 2500 nm using a Shimadzu UV3100 spectrophotometer equipped with an integrating sphere attachment. The Kubelka-Munk function was used to convert diffuse reflectance data to absorption spectra.[31]

Results and Discussion

Synthesis of Ln/Ln'/Q using Sb_2Q_3 fluxes (Q = S, Se). The proven method of using Sb_2Q_3 (Q = S, Se) fluxes to prepare ternary interlanthanide chalcogenides has been very effective in this present study. Eight different structure types have been identified for ternary interlanthanide chalcogenides prepared by employing these fluxes at 1000 °C. These compounds are given in Tables 2 and 3. The structures of Ln/Ln'/Q phases depend highly on the choices of Ln and Ln'. This is especially true for La/Ln'/Se, which can adopt five different structures with the variation of Ln'. It is important to note that the

choices of flux and temperature could be critical as well, which will not be discussed here. Ordered phases can usually be found in bottom left corner of tables, where Ln and Ln' ions have larger difference in size. When it reaches to the opposite corner, disordered compounds are often present owing to the similar structural chemistry of lanthanides. There are some exceptions, e.g. $LaLu_3S_6$ and $La_xYb_{5-x}Se_7$. The limitations of using Sb_2Q_3 (Q = S, Se) fluxes to prepare LnLn'Q include: 1) Attempts to prepare interlanthanide tellurides have not succeeded; 2) It is difficult to achieve high yield and high quality single crystals when the ionic radii of the two Ln^{3+} ions approach equality; 3) Occasionally, distinguishing and separating products from Sb_2Q_3 (Q = S, Se) fluxes proves tricky.

Structures of $Ln_xLu_ySe_z$ (Ln = La, Ce, Pr, Nd, Sm, Gd). The Ln_3LuSe_6 (Ln = La, Ce) compounds adopt U_3ScS_6[32] type structure. The unit cell of La_3LuSe_6, projected along the *c* axis, is shown is Figure 1. There are three crystallographically unique Ln sites (4*g*) and two octahedral Lu positions (2*d*, 2*b*) in the structure. Both Ln(1) and Ln(2) atoms are surrounded by eight Se atoms and occur as bicapped trigonal prism. Ln(3) sites are seven-coordinate in a monocapped trigonal prismatic environment. $LnSe_8$ and $LnSe_7$ polyhedra share faces or edges with each other to form two-dimensional slabs extending in the [*ac*] plane. Furthermore these slabs connect at Se(4) positions to produce a three-dimensional structure. The gaps between these slabs are filled by isolated one-dimensional edge-sharing $LuSe_6$ octahedral chains running down the *c* axis. The bond distances for these two compounds, which can be found in Supporting Information, are normal compared to average values reported by Shannon.[35] In the case of La_3LuSe_6, the bond distances for the $LaSe_8$, $LaSe_7$, and $LuSe_6$ polyhedra range from

2.9982(8) to 3.3408(11) Å, 2.9229(11) to 3.1116(11) Å, and 2.6629(9) to 2.8257(6) Å, respectively.

The series of β-$LnLuSe_3$ (Ln = Pr, Nd) are isotypic with $UFeS_3$.[24] The structure, as shown in Figure 2, is constructed from two-dimensional $LuSe_6$ octahedra layers, which are separated by Ln^{3+} ions. The local environment of Ln^{3+} ions can be found in Figure 5. They coordinate to eight Se atoms with a bicapped trigonal prismatic geometry. The connectivities within $LuSe_6$ layers are illustrated in Figure 3. The $LuSe_6$ octahedral units are edge sharing along *a* axis and corner sharing along *c* axis. The bond lengths within these two compounds are regular. For example, Pr-Se and Lu-Se distances in compound β-$PrLuSe_3$ are in the range of 2.9035(18) and 3.3670(17) Å, and 2.7102(10) and 2.8072(11) Å, respectively.

$Sm_{1.82}Lu_{2.18}Se_6$ and $Gd_{1.87}Lu_{2.13}Se_6$ crystallize in F-Ln_2S_3[25,26] type structure, which was detailed in one of our previous papers.[22] As shown in Figure 4, the eight-coordinate bicapped trigonal prismatic Ln(1) ions (Figure 5) sit in the one-dimensional channels formed by three different double chains via edge- and corner- sharing. These double chains, all running down the *b* axis, are constructed from $Ln(2)Se_7$ monocapped trigonal prisms, $Ln(3)Se_6$ octahedra, and $Ln(4)S_6$ octahedra, respectively. Within each double chain, the building polyhedra share edges with each other both in the direction of chain propagation and with adjacent chains. For $Sm_{1.82}Lu_{2.18}Se_6$, the average distances for $Ln(1)S_8$, $Ln(2)Se_7$, $Ln(3)Se_6$, and $Ln(4)Se_6$ polyhedra are 3.0406(10) Å, 2.9230(10) Å, 2.8064(10) Å, and 2.7791(9) Å, respectively, which are comparable to Shannon's data,[35] 3.05 Å for $SmSe_8$, 3.00 Å for $SmSe_7$, 2.90 Å for $LuSe_7$, and 2.84 Å for $LuSe_6$.

Magnetic Susceptibility. Figure 6 shows the temperature dependence of the inverse molar magnetic susceptibilities for β-$LnLuSe_3$ (Ln = Pr, Nd). Both compounds are paramagnetic and deviate from the Curie-Weiss law below 40 K. The effective magnetic moment and Weiss constant were obtained by fitting the high temperature susceptibility data into the Curie-Weiss law. As shown in Table 4, the effective magnetic moments are close to calculated values for free Ln^{3+} ions. The negative θ_p values indicate antiferromagnetic coupling between magnetic ions.

The magnetic susceptibility of $Sm_{1.82}Lu_{2.18}Se_6$ shows a typical van Vleck paramagnetic behavior similar to Sm metal, which is displayed in Figure 7. There is no magnetic transition down to 2 K and susceptibility data does not follow the Curie-Weiss law. The difference between the ground state ($^6H_{5/2}$) and the first excited state ($^6H_{7/2}$) of Sm^{3+} is not large compared to thermal energy (k_BT). Therefore, the excited states make significant contributions to the magnetic susceptibility at high temperature.[37] The experimental effective magnetic moment of Sm^{3+} can be determined approximately using $\mu_{eff} = [\ 3k_B\chi_m T/(L\mu_0\mu_B^2)]^{1/2}$, where k_B is Boltzmann constant, L is Avogadro's number, μ_0 is vacuum permeability, T is temperature in Kelvin, χ_m is molar susceptibility. At T = 300 K, μ_{eff} = 1.02 μB, which is smaller than the calculated value (1.55 μB) for free Sm^{3+} ions using van Vleck formula.[37] It is probably caused by crystal-field effects.

The magnetic susceptibility of $Gd_{1.87}Lu_{2.13}Se_6$ obeys the Curie-Weiss law above the temperature around 4 K where it undergoes a sharp antiferromagnetic transition, as shown in Figure 8. The effective magnetic moment and Weiss constant were obtained to be 11.77(1) μ_B per formula unit and -4.4(4) K. The magnetization measurement was performed at 2 K and the results are presented in Figure 9. The saturation moment per

Gd^{3+} ion is 7.5 μ_B, which is close to the value for free Gd^{3+} ion (7.94 μ_B) assuming $g = 2$. There is a weak spin reorientation transition at approximately H = 0.5 T.

Ce_3LuSe_6 shows a deviation from the Curie-Weiss law near 70 K owing to crystal-field effects. A magnetic transition was observed below 5 K, which is illustrated in Figure 10. A small divergence on the ZFC-FC measurements (Figure 11) below this temperature may indicate a ferromagnetic component of the transition or owing to a small temperature difference. In order to investigate the magnetic transition in detail, the magnetization measurements at 2 K were conducted as well. Figure 12 shows the field-dependent magnetizations for Ce_3LuSe_6. M(H) increases abruptly at low field, which is consistent with ferromagnetic behavior. The saturation moment per Ce^{3+} ion (1.13 μ_B) is substantially smaller than the moment for free Ce^{3+} ion (2.54 μ_B) assuming $g = 6/7$. It may be because of cystal-field splitting of ground state of Ce^{3+} ion ($^2F_{5/2}$). No magnetic hysteresis was found at 2 K that is consistent with the behavior for a soft ferromagnet. In contrast, the Weiss constant for Ce_3LuSe_6 was determined to be -20(1) K indicating antiferromagnetic interactions between Ce^{3+} ions. It is worth noting that $|\theta_p|$ value may be enlarged due to the crystal-field splitting of the full J=5/2 multiplet for the Ce^{3+}. To conclude, Ce_3LuSe_6 orders ferromagnetically with a weak antiferromagnetic component that might be due to canted spins of Ce^{3+}.

Optical Properties. There are few interlanthanide selenides reported in the literatures. $SmEr_3Se_6$, a red compound, was determined to be a wide direct semiconductor with a band gap of 2.0 eV.[20] The series of compounds, β-$LnYbSe_3$ (Ln = La, Ce, Pr, Nd, Sm), are black in color, as are the title compounds.[14] The UV-vis-NIR diffuse reflectance spectra (Fig. 13) of $Ln_xLu_ySe_z$ (Ln = La, Ce, Pr, Nd, Sm, Gd) reveal

band gaps for La_3LuSe_6, Ce_3LuSe_6, β-$PrLuSe_3$, β-$NdLuSe_3$, $Sm_{1.82}Lu_{2.18}Se_6$, and $Gd_{1.87}Lu_{2.13}Se_6$ of 1.26, 1.10, 1.56, 1.61, 1.51, and 1.56 eV, respectively. The more condensed structure that Ln_3LuSe_6 (Ln = La, Ce) adopt may be the reason for their considerably smaller gaps compared to the Pr, Nd, Sm, and Gd contained phases. The smaller value for Ce_3LuSe_6 is due to the relatively low energy of the $4f^1 \rightarrow 4f^05d^1$ transition for cerium. The fine-structure observed in the spectra for β-$PrLuSe_3$, β-$NdLuSe_3$, and $Sm_{1.82}Lu_{2.18}Se_6$ is actually due to f-f transitions within the lanthanide ions.

Conclusions

Molten Sb_2Q_3 (Q = S, Se) fluxes have been a valuable media to access ternary interlanthanide chalcogenides. The composition and structure of the products depends highly on the choices of lanthanides and chalcogenides. In this present study, we detailed the synthesis of lutetium-based interlanthanide selenides $Ln_xLu_ySe_z$ (Ln = La, Ce, Pr, Nd, Sm, Gd) using a Sb_2Se_3 flux. All of these compounds show diverse structures and physical properties as a function of the Ln ions. They adopt three different structures types including U_3ScS_6 for Ln = La and Ce, $UFeS_3$ for Ln = Pr and Nd, and F-Ln_2S_3 for Ln = Sm and Gd. Ln_3LuSe_6 (Ln = La, Ce) have a very condensed three-dimensional structure that is constructed from two-dimensional $^2_\infty[Ln_3Se_6]^{3-}$ slabs with the gaps between these slabs filled by octahedral Lu^{3+} ions. The structure of β-$LnLuSe_3$ (Ln = Pr, Nd) includes two-dimensional $LuSe_6$ octahedra layers that are separated by eight-coordinate larger Ln^{3+} ions, whereas $Sm_{1.82}Lu_{2.18}Se_6$ and $Gd_{1.87}Lu_{2.13}Se_6$ have a three-dimensional channel structure. Magnetic measurements have shown that both β-$PrLuSe_3$ and β-$NdLuSe_3$ are Curie-Weiss type paramagnets. $Sm_{1.82}Lu_{2.18}Se_6$ exhibits van Vleck

paramagnetism. $Gd_{1.87}Lu_{2.13}Se_6$ was found to have an antiferromagnetic transition around 4 K; whereas Ce_3LuSe_6 has ferromagnetic ordering with a weak antiferromagnetism below 5 K. $Ln_xLu_ySe_z$ (Ln = La, Ce, Pr, Nd, Sm, Gd) are semiconductors with tunable band gaps.

Acknowledgment. This work was supported by the U.S. Department of Energy under Grant DE-FG02-02ER45963 through the EPSCoR Program. Funds for purchasing the UV-vis-NIR spectrometer used in these studies were provided through the Chemical Sciences, Geosciences and Biosciences Division, Office of Basic Energy Sciences, Office of Science, Heavy Elements Program, U.S. Department of Energy under Grant DE-FG02-01ER15187. JSB and ESC acknowledge support from NSF-DMR 0203532. A portion of this work was performed at the National High Magnetic Field Laboratory, which is supported by the National Science Foundation Cooperative Agreement No. DMR-0084173, by the State of Florida, and by the Department of Energy.

Supporting Information Available: X-ray crystallographic files in CIF format for Ln_3LuSe_6 (Ln = La, Ce), β-$LnLuSe_3$ (Ln = Pr, Nd), and $Ln_xLu_{4-x}Se_6$ (Ln = Sm, Gd; x = 1.82, 1.87). This material is available free of charge via the Internet at http://pubs.acs.org. Selected bond distances for Ln_3LuSe_6 (Ln = La, Ce), β-$LnLuSe_3$ (Ln = Pr, Nd), and $Ln_xLu_{4-x}Se_6$ (Ln = Sm, Gd; x = 1.82, 1.87) are also available in summary tables (S1, S2, and S3). Magnetization data for β-$LnLuSe_3$ (Ln = Pr, Nd), and $Sm_{1.82}Lu_{2.18}Se_6$ are also provided.

References

1) Moreau, J. M. *Mater. Res. Bull.* **1968**, *3*, 427.

2) Moreau, J. M.; Mareschal, J.; Bertaut, E. F. *Solid State Commun.* **1968**, *6*, 751.

3) Mareschal, J.; Moreau, J. M.; Ollivier, G.; Pataud, P.; Sivardiere, J. *Solid State Commun.* **1969**, ***7,*** 669.

4) Rodier, N.; Laruelle, P. *C. R. Seances Acad. Sci. Ser. C* **1970**, *270*, 2127.

5) Coutures, J.; Coutures, J. P. *J. Solid State Chem.* **1976**, *19*, 29.

6) Müller-Buschbaum, H.; Graebner, P. -H. *Z. Anorg. Allg. Chem.* **1971**, *386*, 158.

7) Ijdo, D. J. W. *Acta Crystallogr. B* **1980**, *36*, 2403.

8) Ito, K.; Tezuka, K.; Hinatsu, Y. *J. Solid State Chem.* **2001**, *157*, 173.

9) Deepa, M.; Varadaraju, U. V. *Mater. Res. Soc. Symp. Proc.* **1998**, *527*, 507.

10) Berndt, U.; Maier, D.; Keller, C. *J. Solid State Chem.* **1976**, *16*, 189.

11) Ito, K.; Tezuka, K.; Hinatsu, Y. *J. Solid State Chem.* **2001**, *157*, 173.

12) Rodier, N.; Julien, R.; Tien, V. *Acta Crystallogr. C* **1983**, *39*, 670.

13) Carre, D.; Laruelle, P. *Acta Crystallogr. B* **1974**, *30*, 952.

14) Mitchell, K.; Somers, R. C.; Huang, F. Q.; Ibers, J. A. *J. Solid State Chem.* 2004, *177*, 709.

15) Jin, G. B.; Choi, E. S.; Guertin, R. P.; Brooks, J. S.; Bray, T. H.; Booth, C. H.; Albrecht-Schmitt, T. E. *Chem. Mater.* **2007**, *19*, 567.

16) Rodier, N.; Tien, V. *C. R. Seances Acad. Sci. Ser. C* **1974**, *279*, 817.

17) Rodier, N.; Firor, R. L.; Tien, V.; Guittard, M. *Mater. Res. Bull.* **1976**, *11*, 1209.

18) Rodier, N. *Bull. Soc. Fr. Mineral. Cristallogr.* **1973**, *96*, 350.

19) Carré, D.; Laruelle, P. *Acta Cryst.* 1973, *B 29*, 70.

20) Gray, D. L.; Rodriguez, B. A.; Chan, G. H.; Van Duyne, R. P.; Ibers, J. A. *J. Solid State Chem.* in press.

21) Jin, G. B.; Choi, E. S.; Guertin, R. P.; Brooks, J. S.; Bray, T. H.; Booth, C. H.; Albrecht-Schmitt, T. E. *J. Solid State Chem.* in press.

22) Jin, G. B.; Choi, E. S.; Guertin, R. P.; Brooks, J. S.; Bray, T. H.; Booth, C. H.; Albrecht-Schmitt, T. E. *$PrLnYb_2S_6$ (Ln = Tb, Dy); J. Solid State Chem.* submitted.

23) Marezio, M.; Remeika, J. P.; Dernier, P. D. *Acta Crystallogr. B* **1970**, *26*, 2008.

24) Noel, H.; Padiou, J. *Acta Crystallogr. B* **1976**, *32*, 1593.

25) Schleid, T.; Lissner, F. *J. Alloys Compd.* **1992**, *189*, 69.

26) Fang, C. M.; Meetsma, A.; Wiegers, G. A. *J. Alloys Compd.* **1993**, *201*, 255.

27) Zachariasen, W.H. *Acta Crystallogr.* **1949**, *2*, 291.

28) Sheldrick, G. M. *SHELXTL PC, Version 6.12, An Integrated System for Solving, Refining, and Displaying Crystal Structures from Diffraction Data*; Siemens Analytical X-Ray Instruments, Inc.: Madison, WI, 2001.

29) Sheldrick, G. M. *SADABS 2001, Program for absorption correction using SMART CCD based on the method of Blessing: Blessing, R. H. Acta Crystallogr.* **1995**, *A51*, 33.

30) Mulay, L. N.; Boudreaux, E. A. *Theory and Applications of Molecular Diamagnetism*; Wiley-Interscience: New York, 1976.

31) Wendlandt, W. W.; Hecht, H. G. *Reflectance Spectroscopy*; Interscience Publishers: New York, 1966.

32) Rodier, N.; Tien, V. *Acta Crystallogr.* **1976**, *32*, 2705.

33) Becker, D. F.; Kasper, J. S. *Acta Crystallogr.* **1957**, *10*, 332.

34) Adolphe, C. *Annales de Chimie (Paris)* **1965**, *10*, 271.

35) Shannon, R. D. *Acta Cryst.***1976**, *A32*, 751.

36) Kittel, C. *Introduction to Solid State Physics*, 6th Ed., Wiley, New York, 1986.

37) Van Vleck, J. H. *The Theory of Electric and Magnetic Susceptibilities*; Oxford University Press: London, 1932.

Table 1. Crystallographic Data for $Ln_xLu_ySe_z$ (Ln = La, Ce, Pr, Nd, Sm, Gd).

Formula	La_3LuSe_6	Ce_3LuSe_6	β-$PrLuSe_3$	β-$NdLuSe_3$	$Sm_{1.82}Lu_{2.18}Se_6$	$Gd_{1.87}Lu_{2.13}Se_6$
fw	1065.46	1069.09	552.76	556.09	1128.83	1140.50
Color	black	black	black	black	black	black
Crystal System	orthorhombic	orthorhombic	orthorhombic	orthorhombic	monoclinic	monoclinic
Space group	*Pnnm* (No. 58)	*Pnnm* (No. 58)	*Cmcm* (No. 63)	*Cmcm* (No. 63)	$P2_1/m$ (No. 11)	$P2_1/m$ (No. 11)
a (Å)	14.6195(10)	14.5020(9)	4.0052(10)	3.9946(5)	11.3925(13)	11.4274(12)
b (Å)	17.5736(12)	17.4954(11)	12.996(3)	13.0015(17)	4.0483(5)	4.0542(4)
c (Å)	4.1542(3)	4.1129(3)	9.865(3)	9.8583(13)	11.6844(14)	11.7160(12)
β					108.915(2)	109.005(2)
V (Å^3)	1067.29(13)	1043.52(12)	513.5(2)	512.00(11)	509.79(11)	513.20(9)
Z	4	4	4	4	2	2
T (K)	193	193	193	193	193	193
λ (Å)	0.71073	0.71073	0.71073	0.71073	0.71073	0.71073
ρ_{calcd} (g cm^{-3})	6.631	6.805	7.150	7.214	7.354	7.381
μ (cm^{-1})	413.24	430.70	495.66	503.36	525.94	534.34
R(F)[a]	0.0273	0.0212	0.0429	0.0226	0.0300	0.0308
$R_w(F_o^2)$ [b]	0.0645	0.0485	0.1049	0.0601	0.0822	0.0817

[a] $R(F) = \sum \left| |F_o| - |F_c| \right| / \sum |F_o|$ for $F_o^2 > 2\sigma(F_o^2)$. [b] $R_w\left(F_o^2\right) = \left[\sum \left[w\left(F_o^2 - F_c^2\right)^2 \right] / \sum wF_o^4 \right]^{1/2}$.

Table 2. Ternary Interlanthanide Sulfides Prepared Using Sb_2S_3 flux at 1000 °C.

	Eu^{2+}	La^{3+}	Ce^{3+}	Pr^{3+}	Nd^{3+}	Sm^{3+}	Gd^{3+}
Tb^{3+}	●						
Dy^{3+}	●	◙Δ					
Ho^{3+}	●	◙Δ	◊				
Er^{3+}	●	◙	◙				
Tm^{3+}	●	◙	◙	Δ			
Yb^{3+}	●	◙	◙	Δ	Δ	Δ	Δ
Lu^{3+}	●	Δ	◊	◊	◊	Δ	

Table 3. Ternary Interlanthanide Selenides Prepared Using Sb_2Se_3 flux at 1000 °C.

	Eu^{2+}	La^{3+}	Ce^{3+}	Pr^{3+}	Nd^{3+}	Sm^{3+}	Gd^{3+}
Tb^{3+}	●	□					
Dy^{3+}	●		□				
Ho^{3+}	●						
Er^{3+}	●	◊			Δ		
Tm^{3+}	●	Δ	Δ	Δ	Δ	Δ	Δ
Yb^{3+}	●	○	▲	▲	▲	Δ	Δ
Lu^{3+}	●	■	■	▲	▲	Δ	Δ

Ordered structure types: ▲ β-$LnLn'S_3$,[12-14] ◙ γ- $LnLn'S_3$,[15] ■ U_3ScS_6,[32] ● $CaFe_2O_4$.[33]
Disordered structure types: Δ F-Ln_2S_3,[25,26] ◊ δ-$LnLn'S_3$,[18,21] □ U_2S_3,[27] ○ Y_5S_7.[34]

Table 4. Magnetic Parameters for $PrLnYb_2S_6$ (Ln = Pr/Yb, Tb, Dy).

Formula	P_{cal}/μ_B	P_{eff}/μ_B	θ_p/K	R^2
Ce_3LuSe_6	4.40	4.56(1)	-20(1)	0.99959
β-$PrLuSe_3$	3.58	3.509(3)	-15.6(4)	0.99993
β-$NdLuSe_3$	3.62	3.913(9)	-25(1)	0.99961
$Gd_{1.87}Lu_{2.13}Se_6$	10.86	11.77(1)	-4.4(4)	0.99991

[a] P_{cal} and P_{eff} : calculated [36] and experimental effective magnetic moments per formula unit.
[b] Weiss constant (θ_p) and goodness of fit (R^2) obtained from high temperature (100-300 K) data.

Figure Captions

Figure 1. An illustration of the three-dimensional structure of La_3LuSe_6 down the *c* axis.

Figure 2. Unit cell of β-$PrLuSe_3$ viewed along the *a* axis. Pr-Se bonds have been omitted for clarity.

Figure 3. A depiction of an individual $LuSe_6$ octahedra layer viewed down the *b* axis in β-$PrLuSe_3$.

Figure 4. A view the three-dimensional channel structure of $Sm_{1.82}Lu_{2.18}Se_6$ along the *b* axis.

Figure 5. Illustrations of the coordination environments for Pr ions in β-$PrLuSe_3$ and Sm(1)/Lu(1) ions in $Sm_{1.82}Lu_{2.18}Se$.

Figure 6. The temperature dependence of the reciprocal molar magnetic susceptibility for β-$PrLuSe_3$ and β-$NdLuSe_3$, under an applied magnetic field of 0.1 T between 2 and 300 K. The straight line represents the fit to Curie-Weiss law in the range of 100-300 K.

Figure 7. Molar magnetic susceptibility vs temperature between 2 and 300 K for $Sm_{1.82}Lu_{2.18}Se_6$. Data were taken under an applied magnetic field of 0.1 T.

Figure 8. Inverse molar magnetic susceptibility vs temperature for $Gd_{1.87}Lu_{2.13}Se_6$ under an applied magnetic field of 0.1 T between 2 and 300 K. The solid line represents the fit to Curie-Weiss law in the range of 100-300 K. Inset shows the molar magnetic susceptibility at low temperature.

Figure 9. The magnetization for $Gd_{1.87}Lu_{2.13}Se_6$ as a function of applied field at 2 K. Inset shows the M(H) curve between 0 and 1 T. Red and green lines are linear fits extended from zero field and from 1T, respectively. Slight increasing of the slope and the weak spin reorientation transition field at the junction (up arrow) can be observed.

Figure 10. Inverse molar magnetic susceptibility as a function of temperature for Ce_3LuSe_6 under an applied magnetic field of 0.1 T between 2 and 300 K. The straight line represents the fit to Curie-Weiss law in the range of 100-300 K. Inset shows the inverse molar magnetic susceptibility at low temperature.

Figure 11. Molar magnetic susceptibility as a function of temperature for Ce_3LuSe_6 under ZFC and FC conditions with an applied magnetic field of 0.01 T between 2 and 25 K.

Figure 12. The magnetization for Ce_3LuSe_6 as a function of applied field at 2 K.

Figure 13. UV-vis diffuse reflectance spectra of $Ln_xLu_ySe_z$ (Ln = La, Ce, Pr, Nd, Sm, Gd).

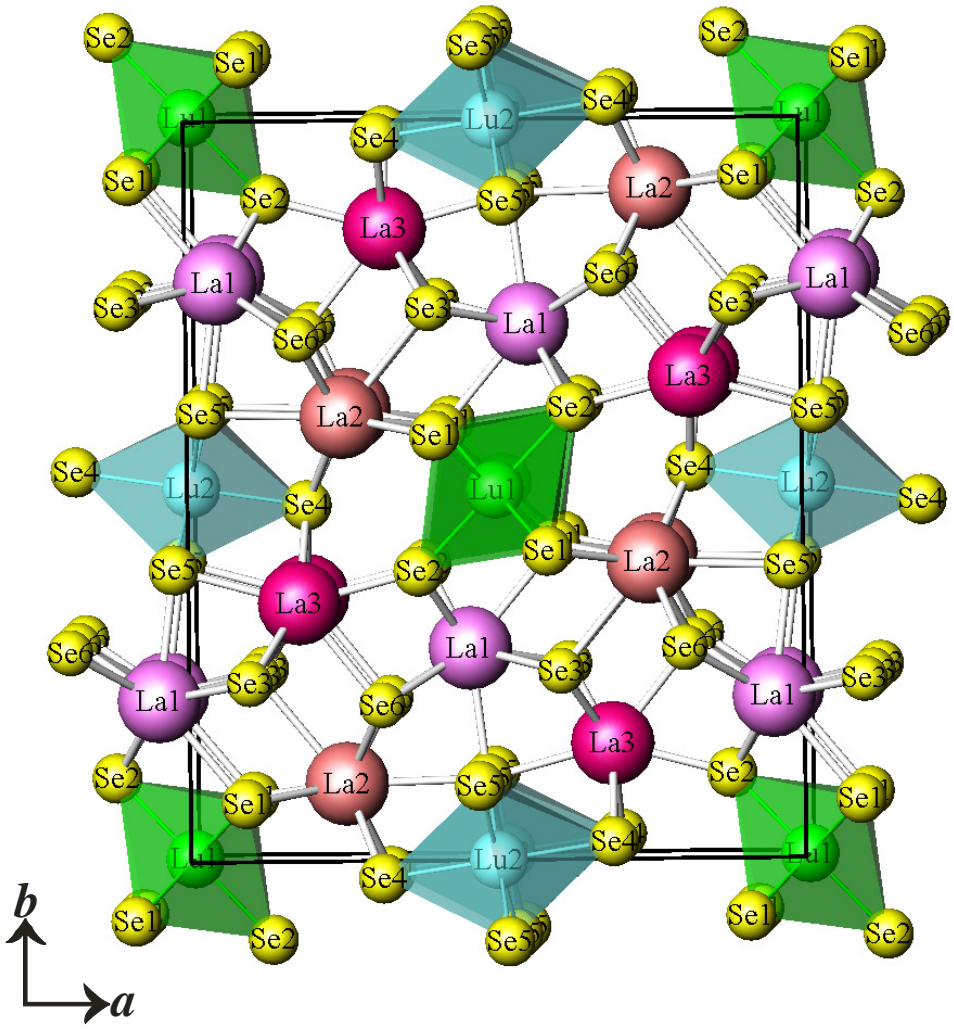

Figure 1

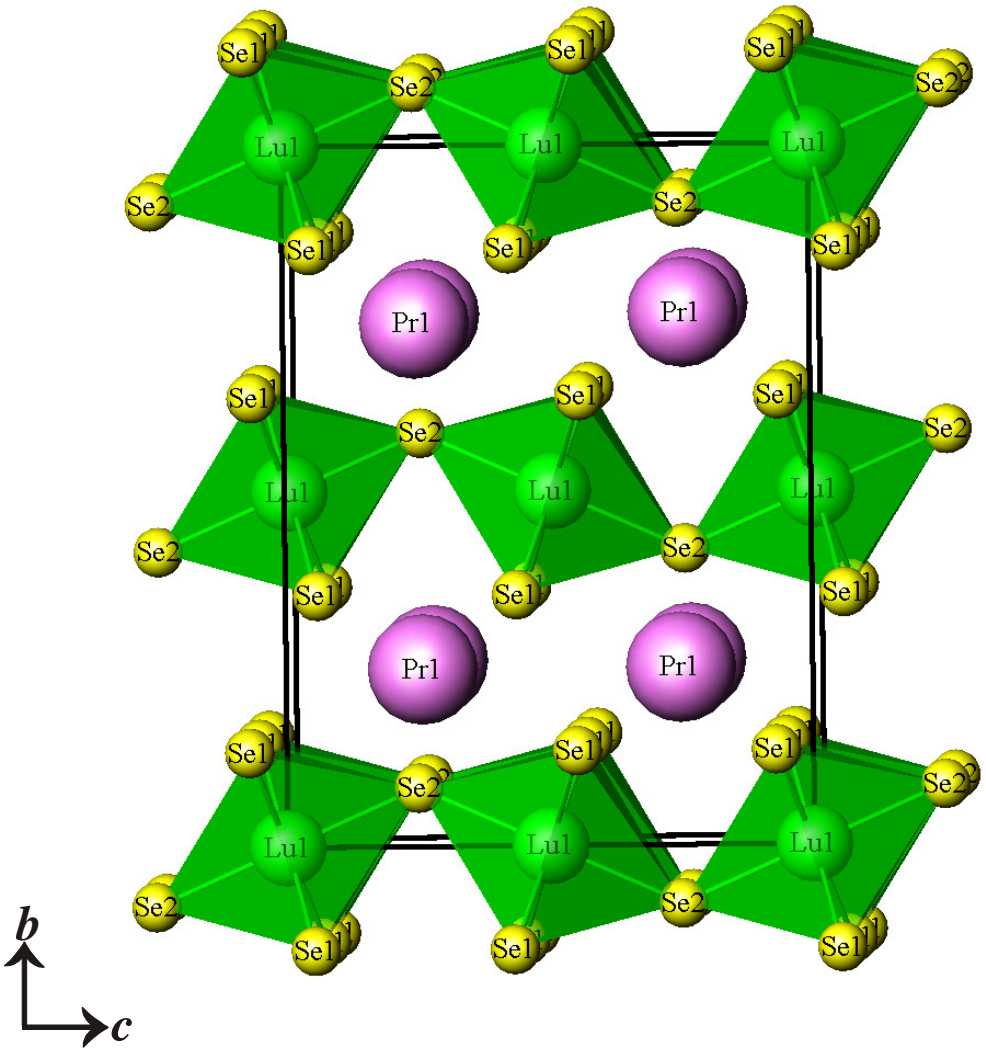

Figure 2

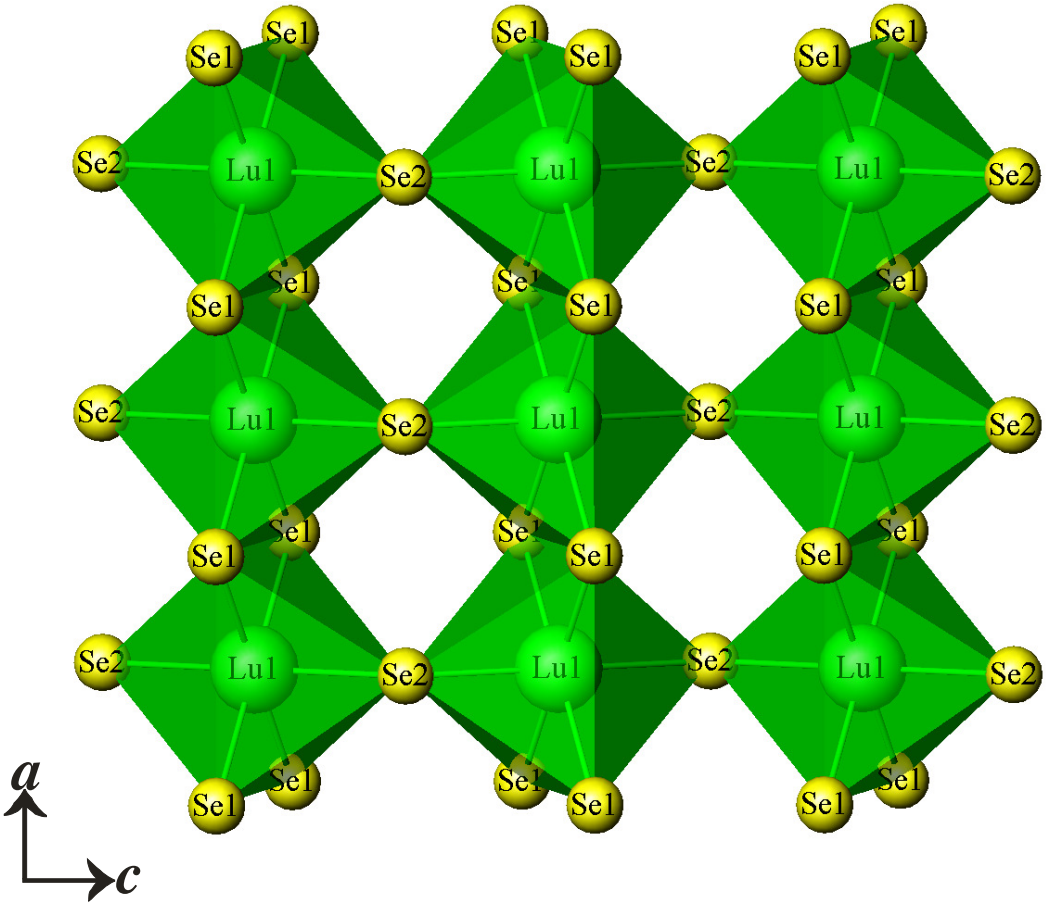

Figure 3

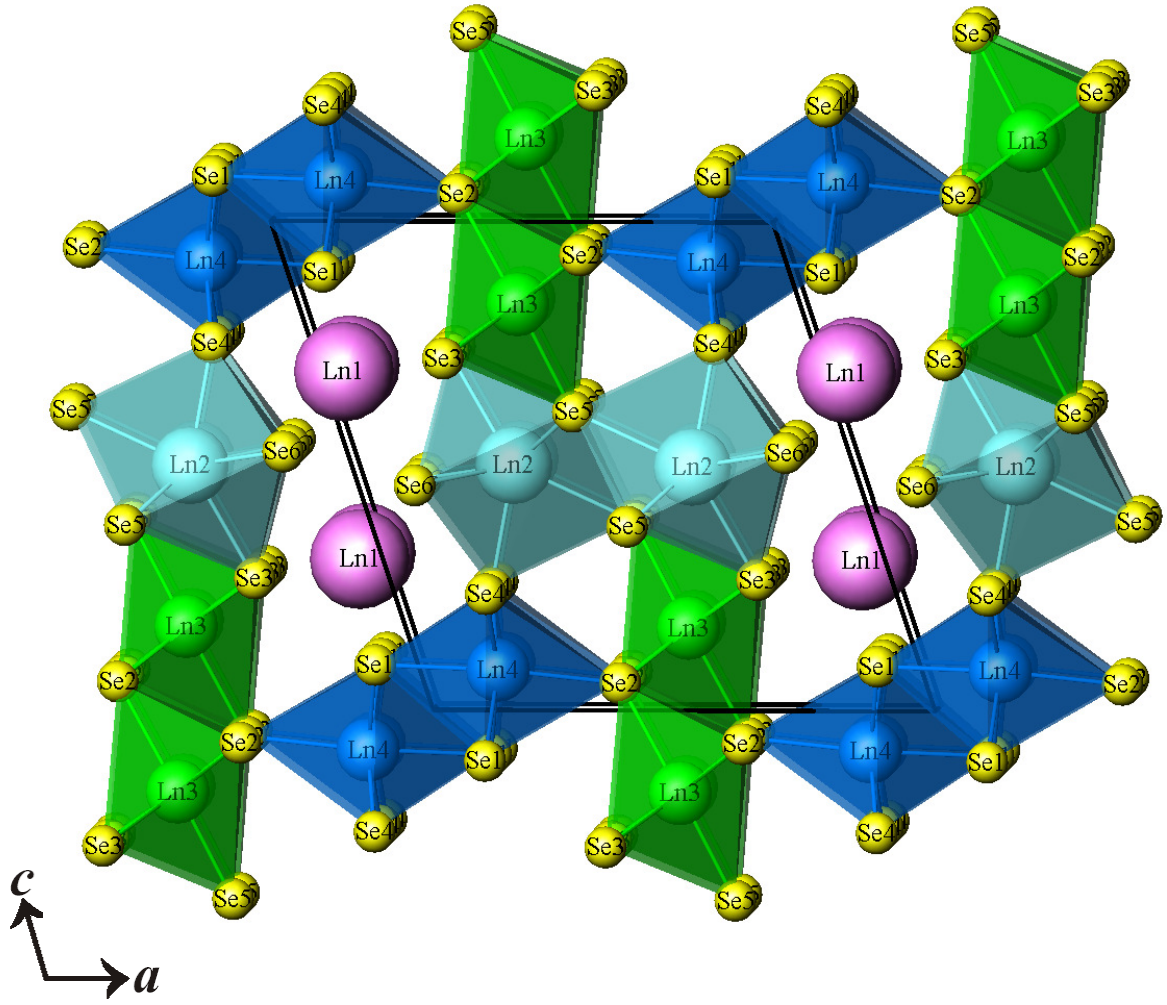

Figure 4

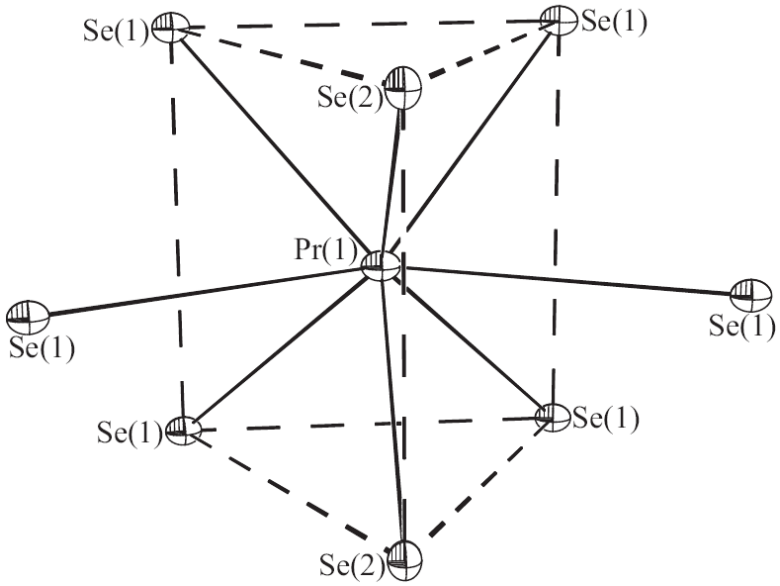
Se(1)
Se(1)
Se(2)
Pr(1)
Se(1)
Se(1)
Se(1)
Se(1)
Se(2)

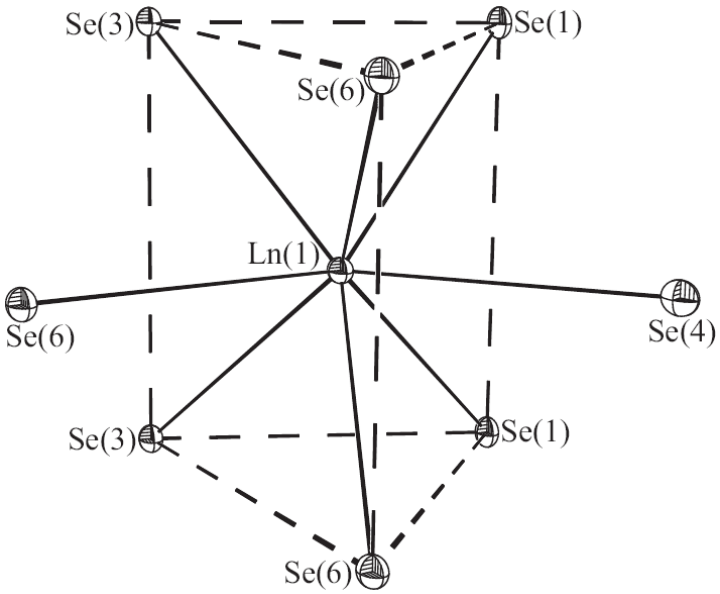
Se(3)
Se(1)
Se(6)
Ln(1)
Se(6)
Se(4)
Se(3)
Se(1)
Se(6)

Figure 5

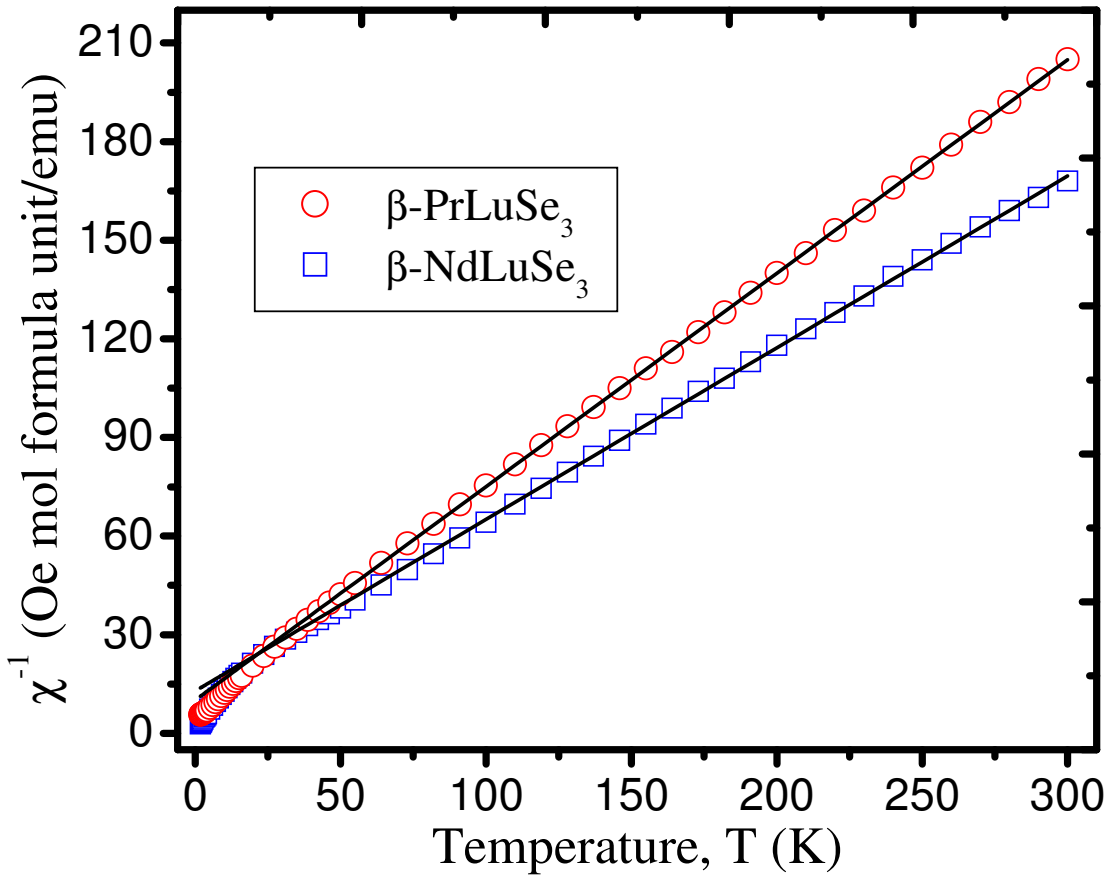
210
180
150
120
90
60
30
0
χ^{-1} (Oe mol formula unit/emu)
β-PrLuSe$_3$
β-NdLuSe$_3$
0
50
100
150
200
250
300
Temperature, T (K)

Figure 6

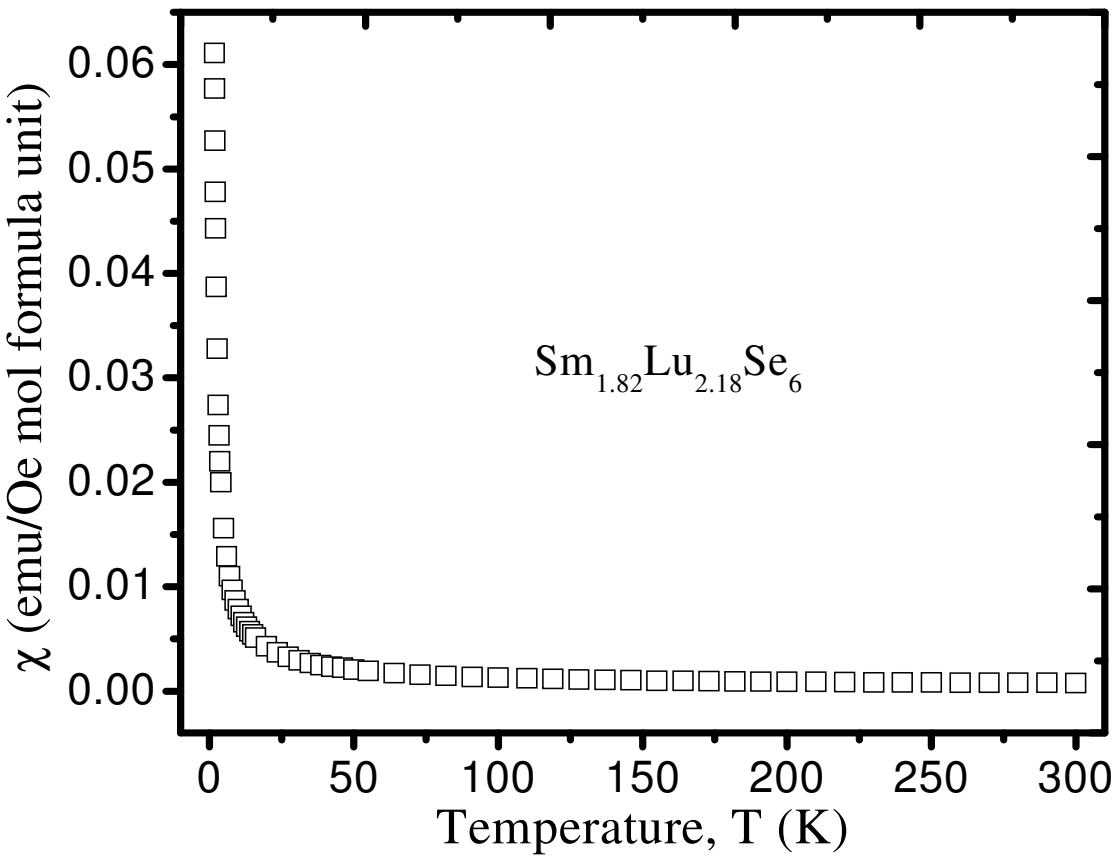
χ (emu/Oe mol formula unit)
0.06
0.05
0.04
0.03
0.02
0.01
0.00
Sm1.82Lu2.18Se6
0
50
100
150
200
250
300
Temperature, T (K)

Figure 7

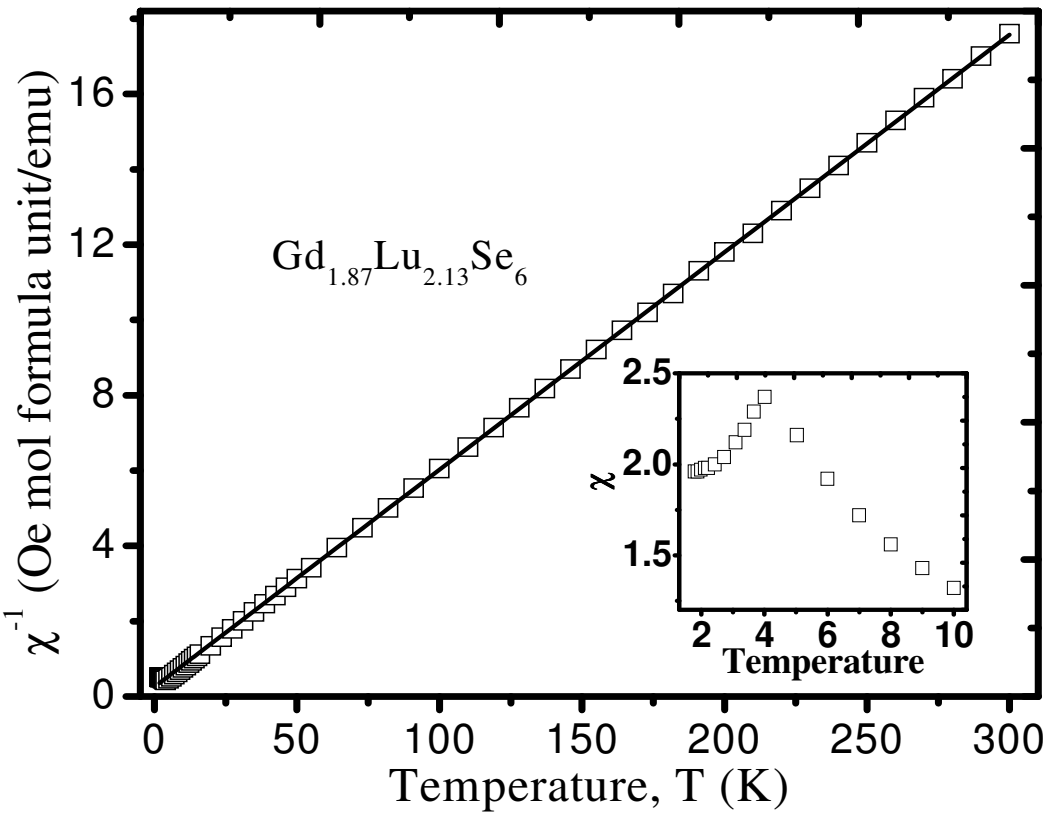
χ^{-1} (Oe mol formula unit/emu)
Temperature, T (K)
$Gd_{1.87}Lu_{2.13}Se_6$
χ
Temperature
0
4
8
12
16
0
50
100
150
200
250
300
1.5
2.0
2.5
2
4
6
8
10

Figure 8

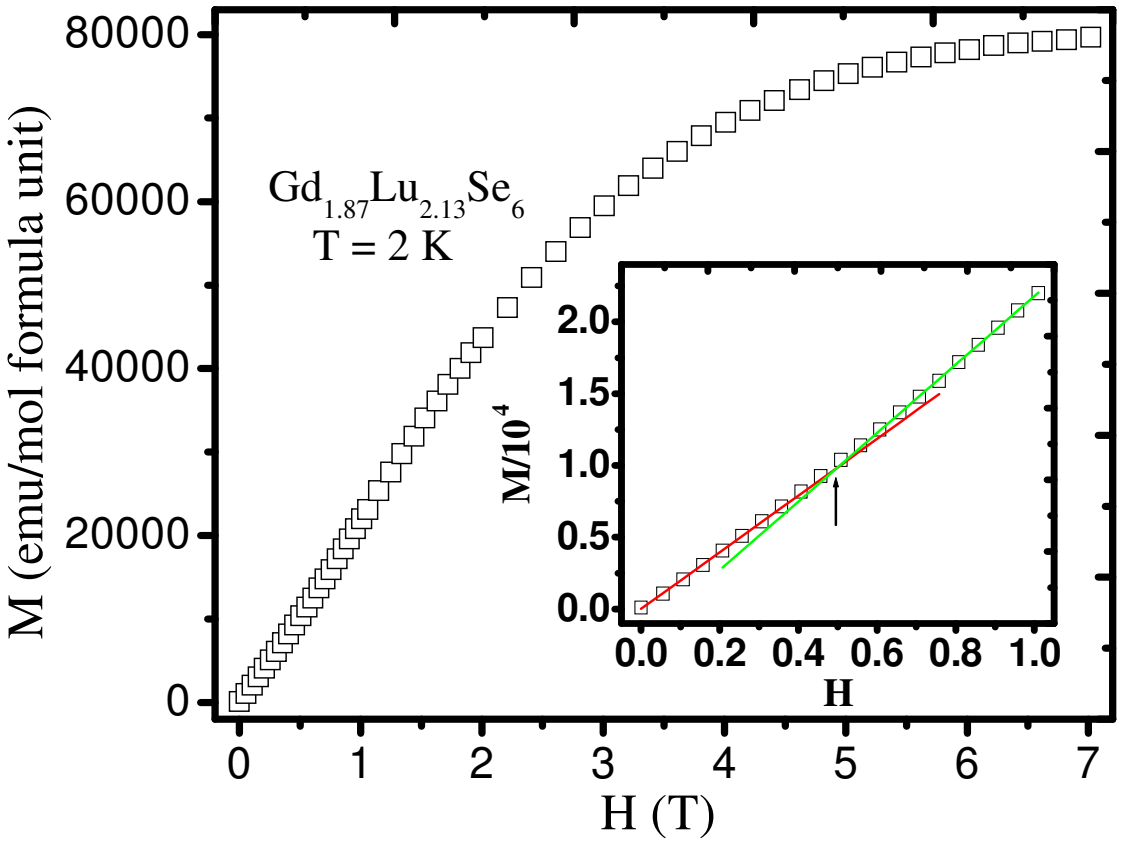
80000
60000
40000
20000
0
M (emu/mol formula unit)
Gd1.87Lu2.13Se6
T = 2 K
0
1
2
3
4
5
6
7
H (T)
M/10^4
2.0
1.5
1.0
0.5
0.0
0.0 0.2 0.4 0.6 0.8 1.0
H

Figure 9

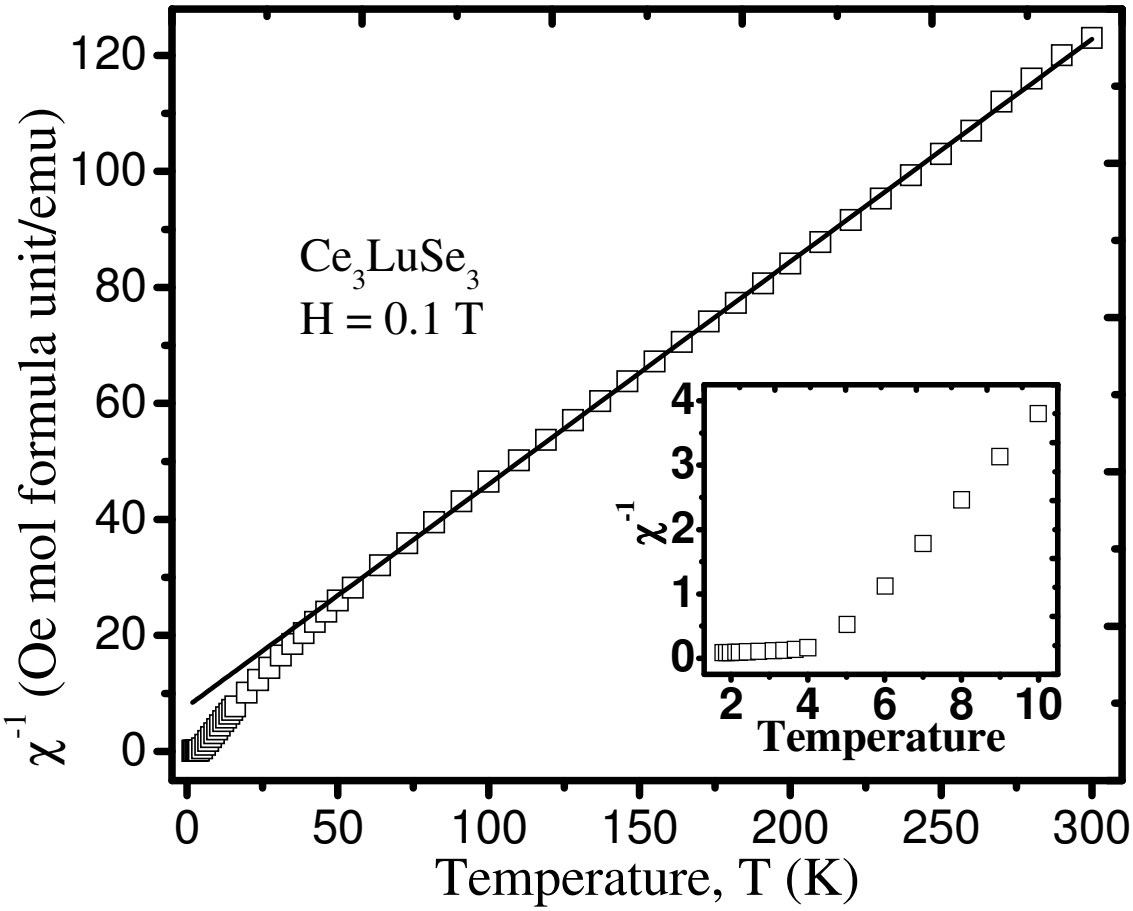
Ce3LuSe3
H = 0.1 T
χ-1 (Oe mol formula unit/emu)
Temperature, T (K)
χ-1
Temperature
0
20
40
60
80
100
120
0
50
100
150
200
250
300
1
2
3
4
2
4
6
8
10

Figure 10

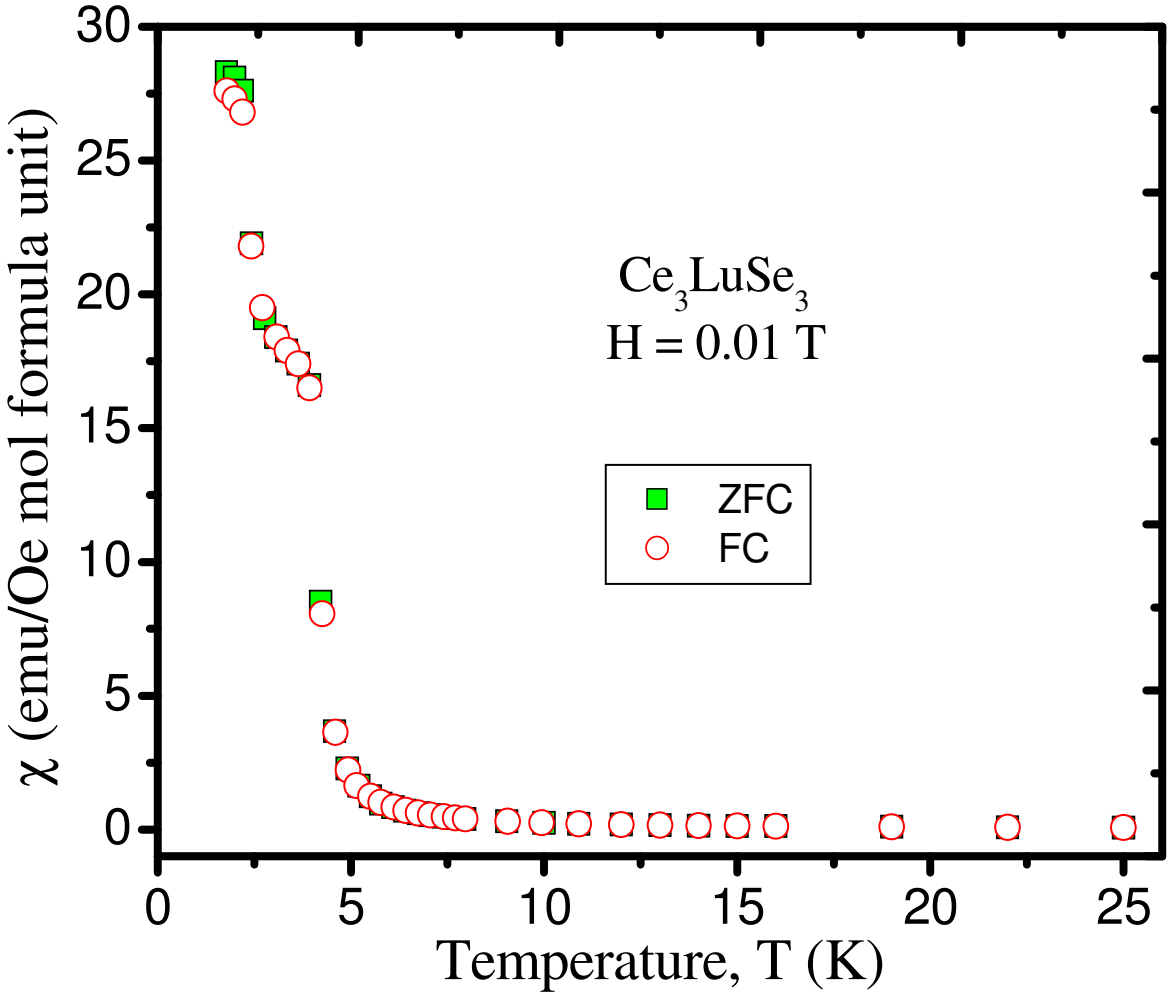
30
25
20
15
10
5
0
χ (emu/Oe mol formula unit)
0
5
10
15
20
25
Temperature, T (K)
Ce3LuSe3
H = 0.01 T
ZFC
FC

Figure 11

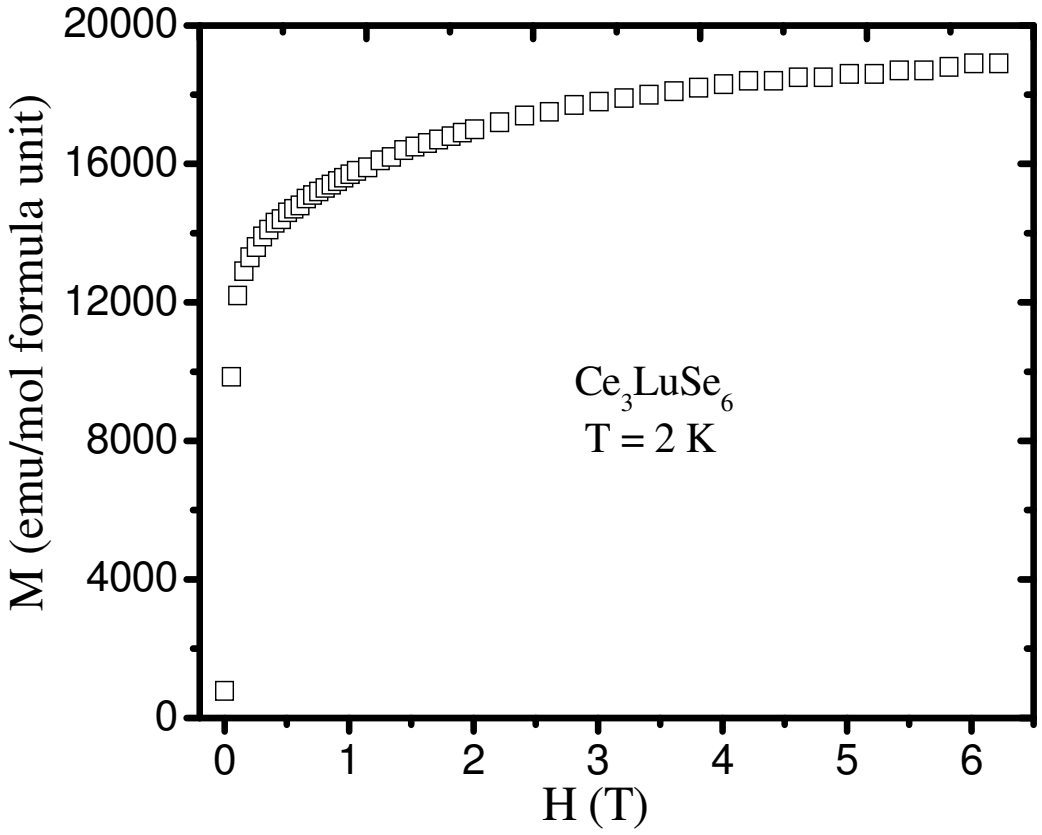
20000
16000
12000
8000
4000
0
M (emu/mol formula unit)
0
1
2
3
4
5
6
H (T)
Ce3LuSe6
T = 2 K

Figure 12

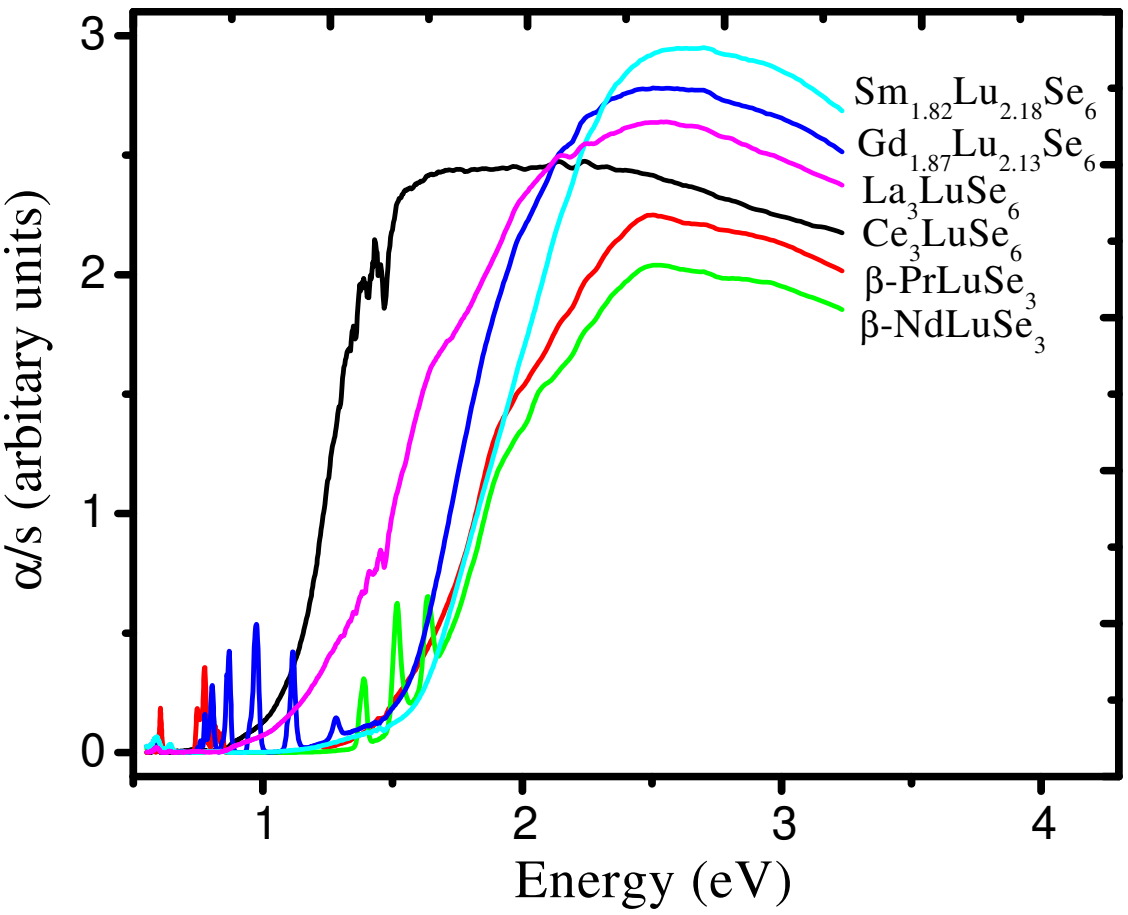
α/s (arbitary units)
Energy (eV)
0
1
2
3
1
2
3
4
Sm1.82Lu2.18Se6
Gd1.87Lu2.13Se6
La3LuSe6
Ce3LuSe6
β-PrLuSe3
β-NdLuSe3

Figure 13